Chemical Engineering Journal 141 (2008) 379–382

Contents lists available at ScienceDirect

Chemical Engineering Journal

journal homepage: www.elsevier.com/locate/cej

Short communication

Effects of gas–solid reaction on liquid defiltration in a MCM-41

Aijie Han, Yu Qiao*

Department of Structural Engineering, University of California - San Diego, 9500 Gilman Drive MC 0085, La Jolla, CA 92093-0085, United States

ARTICLE INFO

Article history:
Received 28 December 2007
Received in revised form 27 February 2008
Accepted 28 February 2008

Keywords:
Nanoporous
Defiltration
Gas–solid reaction

ABSTRACT

Through a pressure-induced infiltration experiment, it is validated that the degree of hydrophobicity of the nanopore surfaces of a MCM-41 can be increased through gas–solid treatment. Compared with the effects of liquid–solid treatment, the infiltration pressure does not vary much while the defiltration pressure is higher, indicating that the reversibility of confined liquid motion is improved; that is, the sorption curve is less hysteretic. The liquid composition and the post-treatment procedure also have considerable influences on the infiltration and defiltration behaviors.

1. Introduction

The field of chemical engineering has been considerably broadened since the last century, partly motivated by the increasingly high functional requirements of advanced materials. For instance, nanoporous materials, which in the past had been widely used for catalysis, absorption and adsorption, and purification and separation, recently found new applications in mechanical structures [1,2]. With controlled surface properties, e.g. if the nanopore surfaces are lyophobic, when a nanoporous material is suspended in a liquid, the nanopores can serve as supporting framework of gas nanophase that is stable under ambient condition. When temperature increases, due to the change in wettability the liquid can infiltrate into the nanopores. If the temperature decreases back, the liquid can defiltrate as the nanopore surface is nonwettable again [3]. Such a system is effectively a thermal machine that works between two different temperatures, converting thermal energy to mechanical work. Because of the large nanopore surface area, the energy density is much larger than that of conventional smart solid materials, such as shape-memory alloys and polymers [4]. It has great potential for active control, microscopic or nanometer-scale actuation, etc.

The system configuration can also be controlled mechanically. At a constant temperature, if the quasi-static pressure, P, in the liquid phase is increased, when the capillary effect is overcome the gas nanophase would vanish, i.e. the liquid molecules are intruded into the nanopores [5,6]. When P is reduced, the defiltration behaviors of the confined liquid are dominated by a number of intrinsic and extrinsic factors [7–9]. Because of the "ink-bottle effect" associated with the irregular nanopore structure [10], the dependence of effective contact angle on liquid motion [11], the energy barrier of vapor phase nucleation and growth [12], and/or the change in gas solubility in nanoenvironment [13], the liquid can be "locked" inside even when the external pressure is entirely removed. When the liquid infiltrates, a large amount of external work must be done to increase the system free energy because the contact area of solid and liquid greatly increases. If the liquid does not defiltrate, the increase in solid–liquid interfacial tension is effectively dissipated, and such a system absorbs energy. For a nanoporous material with the specific nanopore surface area of 10^3 m^2/g and a liquid phase having the excess interfacial tension of 10 to 10^2 mJ/m^2, the energy absorption efficiency is in the range of 10 to 10^2 J/g [14–16], much higher than that of many protection/damping solids [17]. In a number of nanoporous energy absorption systems (NEAS), with the appropriate adjustment of system structures and working conditions, the confined liquid can defiltrate at reduced pressures [18–20]. That is, while the confined liquid does not come out of the nanopores immediately when the pressure is lowered, before P is decreased to zero, the defiltration will occur, resulting in a hysteretic infiltration–defiltration loop. Such a system can work repeatedly as the external loading is applied cyclically, and is attractive for applications such as damping stages, cushioning layers, vibration-resistant containers, etc., where the system performance must be stable in a relatively long period of time.

In order to adjust the defiltration behaviors, the nanopore surfaces must be modified. The external surfaces have little influence on this process, as long as the accessibility of the nanopores is assured. Controlling properties of inner surfaces of a nanoporous material is a nontrivial task. The molecular size of the treatment reagent must be much smaller than the nanopore diameter, otherwise it cannot enter the nanopores even when the solid surface is

* Corresponding author.
E-mail address: yqiao@ucsd.edu (Y. Qiao).

1385-8947/$ – see front matter © 2008 Elsevier B.V. All rights reserved.
doi:10.1016/j.cej.2008.02.025

nominally wettable [21,22]. The treatment time, temperature, and chemical concentrations should be tightly controlled so that the surface reactions can be performed relatively uniformly [23]. In the past, it was shown that through liquid–solid reactions various sorption curves of different infiltration and defiltration characteristics could be obtained [24–27]. In this article, we report the results of an experiment on gas–solid reaction.

2. Experimental

In order to focus on the surface treatment effect, we investigated a commercially available MCM-41 (Sigma–Aldrich No. 643645), with the nanopore diameter of 2.7 nm and the specific surface area of 1040 m^2/g. The material characterization was performed by using a Micromeritics TriStar-3000 Gas Adsorption Analyzer. About 2 g of MCM-41 was placed in a stainless steel cylinder. By using a type 5580 Instron machine, a steel piston was compressed into the cylinder, applying a pressure of 0.3 MPa. Under such a pressure, the MCM-41 powders were close-packed and consolidated into disks. The disks were sealed in a vertical condenser that was connected to a round-bottom flask. Prior to the surface treatment, the system had been dried and was free of moisture. The MCM-41 disks were placed on a bundle of glass wools in between the condenser and the flask. At the top of the condenser, a drying pipe was used to prevent moisture. After adding 10 mL of chlorotrimethylsilane, the flask was heated at 80 °C by a thermal mental for 24 h, so that the MCM-41 sample was exposed to the $(CH_3)_3SiCl$ vapor. Then, the MCM-41 disks were taken out of the condenser and dried in air at room temperature for 6 h or dried in vacuum at 50 °C for 6 h. After the modification, according to a Tristar-3000 gas adsorption analysis, the specific surface area and the pore volume of the dried sample decreased to 692 m^2/g and 0.68 cm^3/g, respectively. For comparison purpose, control samples were also prepared by a liquid–solid reaction method using the same MCM-41. The details of the surface treatment procedure have been discussed elsewhere [28].

The sorption curves were measured by using a pressure-induced infiltration experimental setup. In a stainless steel cylinder, the MCM-41 particles were mixed with a liquid. The liquid phase was either pure water or 26% sodium chloride solution. A steel piston equipped with a reinforced gasket was intruded into the cylinder, driven by a type 5582 Instron machine. The loading rate was kept constant at 1 mm/min. When the pressure, P, reached about 85 MPa, the crosshead of the machine was moved back at the same rate, and P was measured continuously. Typical measurement results are shown in Figs. 1–4, where the pressure is defined as F/A and the system volume change is defined as Ad, with F being the piston force and A and d the cross-sectional area and the displacement of the piston, respectively.

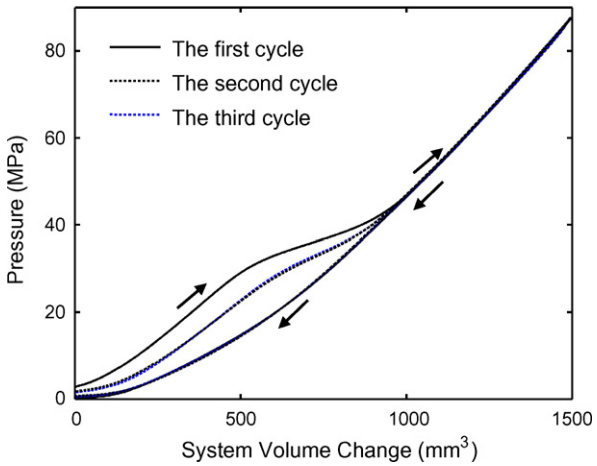

Fig. 2. Typical sorption curves of MCM-41 treated by gas–solid reaction. The liquid phase is distilled water.

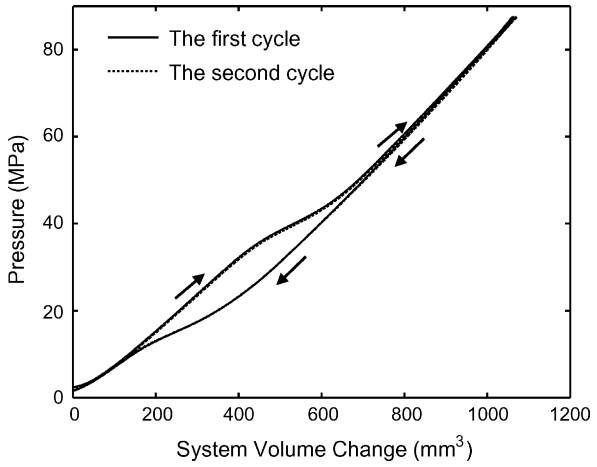

Fig. 3. Typical sorption curves of MCM-41 treated by liquid–solid reaction. The liquid phase is saturated sodium chloride solution.

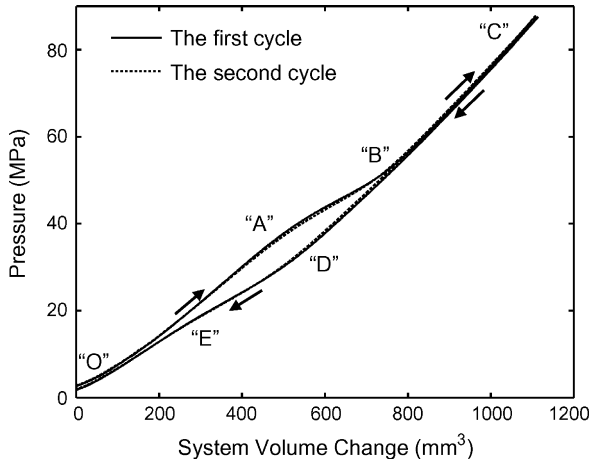

Fig. 1. Typical sorption curves of MCM-41 treated by gas–solid reaction. The liquid phase is saturated sodium chloride solution.

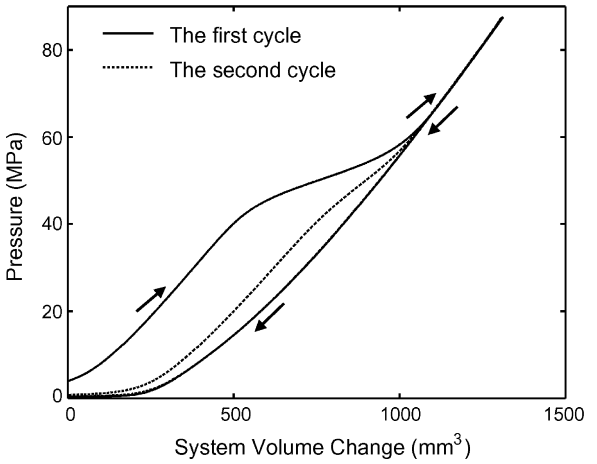

Fig. 4. Typical sorption curves of MCM-41 treated by gas–solid reaction and air dried. The liquid phase is saturated sodium chloride solution.

3. Results and discussion

When the MCM-41 is exposed to the chlorotrimethylsilane vapor at elevated temperature $(CH_3)_3SiCl$ molecules can diffuse into the nanopores and react with the hydroxyl groups at nanopore surfaces. With the byproduct of HCl, which is removed in the drying procedure, the material is silylated with hydrophobic chlorotrimethylsilane [29]. As a result, the nanopore surface becomes nonwettable to the liquid phase. When the treated MCM-41 is immersed in the liquid, no infiltration would take place. As shown by section "OA" in Fig. 1, the gas phase entrapped in the nanopores is stable when the pressure, P, is lower than 38 MPa. In this pressure range, when the piston is intruded in the cylinder, the liquid outside the MCM-41 particles is compressed linearly. Once $P > 38$ MPa, in section "AB", the slope of the sorption curve decreases, which should be attributed to the pressure-induced liquid infiltration [30,31]. That is, with the aid of the external pressure, the liquid molecules can overcome the repelling effect of nanopore surfaces, causing an accelerated system shrinkage. From "B" to "C", the slope of sorption curve increases back to the initial value, indicating that the liquid infiltration is completed. As the pressure is reduced, initially the slope is the same as that of section "BC", as it should be, since the pressure is still high and the liquid is confined in the nanopores. When the pressure decreases to about 30 MPa ("D"), the slope is much lowered, suggesting that defiltration starts. As the vapor phase is restored in the nanopores and the liquid molecules move out, the system expands considerably, causing the formation of a defiltration plateau ("DE"). The slopes of the infiltration plateau and the defiltration plateau are close to each other, which indicates that the liquid motion in nanopores is somewhat reversible, even though the infiltration pressure is higher than the defiltration pressure. Eventually, when all the confined liquid defiltrates, the system configuration changes back to its initial condition, and section "EO" in unloading path overlaps with section "OA" in loading path. When similar loading–unloading procedure is repeated, the same sorption curve can be obtained again, as shown by the dashed line in Fig. 1.

The difference between the infiltration and defiltration pressures, ΔP, reflects the difficulty of defiltration. During infiltration, since the external loading is quasi-static, the work done by the pressure, P, is converted to the excess solid–liquid interfacial tension, which can be regarded as the driving force of defiltration. Upon unloading, the pressure must be over-reduced by about 8 MPa to trigger the defiltration. In the framework of mean-field analysis, the resistance to defiltration can be assessed as $R(2\pi r)$, where R is the work that must be done to overcome the barrier effect of a unit area of nanopore surface and $r = 1.35$ nm is the average nanopore radius. The driving force of liquid motion can be stated as $\Delta P(\pi r^2)$. Thus, $R = \Delta P r/2$, which is about 5 mJ/m^2. According to classic potential functions of solid and liquid molecules [32], the depth of energy well at a silica surface is at the order of 10^{-21} J per molecule. If the number of liquid molecules per nm^2 of nanopore surface is around 10, the resistance to defiltration should be 10 mJ/m^2, comparable with but larger than the measured value. The difference between them may be attributed to the relatively large nanopore size. That is, since the nanopore is much larger than a single liquid molecule, the diffusion along the axial direction can take place after the diffusion along the radius direction, so that the solid–liquid molecular distance is increased and the energy barrier is lowered.

If the liquid phase is pure water, as shown in Fig. 2, the defiltration becomes much more difficult. At the first loading, the defiltration does not start until the pressure is reduced to about 20 MPa. Even after the pressure is entirely removed, there is still a portion of confined liquid that stays inside the nanopores. As a result, at the second loading, the infiltration volume, i.e. the width of the infiltration plateau, is smaller than that in the first cycle. After the second cycle, the sorption curve converges to an equilibrium state and no further variation can be observed as the loading–unloading process is further repeated. Clearly, with the absence of the electrolyte, the resistance to defiltration increases, which may be associated with the structure of solvated ions. The water molecule cluster surrounding a cation tends to move as a whole, and therefore the effective polarity of the liquid phase is lowered, reducing the energy barrier offered by the nanopore surface. For the same reason, the infiltration pressure of the pure water-based system is lower than that of sodium chloride solution-based system. These observations are consistent with the previous experimental results of nanoporous silica gel [33,34].

Compared with the performance of the control sample that is treated by liquid–solid method (Fig. 3), the infiltration pressure of the MCM-41 modified by gas–solid method is similar while the defiltration pressure is higher. The infiltration pressure of the control sample is around 36 MPa, slightly smaller than that shown in Fig. 1 by 5%. The defiltration pressure of the control sample is about 25 MPa, smaller than that in Fig. 1 by 20%. The difference between the infiltration and the defiltration pressures of the control sample is 11 MPa, larger than that in Fig. 1 by nearly 30%. It is clear that the gas–solid treated sample offers better defiltration performance. In the liquid–solid treatment, the MCM-41 particles are immersed in a liquid media. The solvent and the solute molecules diffuse into the nanopores simultaneously. Since the effective viscosity of the solvent is finite, the mobility of chlorotrimethylsilane molecules is smaller than that in vapor phase. However, in the gas–solid treatment, the molecular diffusion rate of chlorotrimethylsilane at the gas–solid interface is much faster compared with that in a liquid–solid modification procedure. Hence, the treatment reagent can diffuse more smoothly in the nanoporous environment, leading to the formation of relatively uniform surface group layers. As the chlorotrimethylsilane groups distribute regularly, the infiltration pressure increases slightly because of the lower defect density. Since defect sites tend to be less hydrophobic, the low defect density also results in the smooth defiltration behavior, which provides additional drag force to water molecules that diffuse along the axial direction. In this case, the defiltration is improved by gas–solid modification, which confirms that the surface functionalization is enhanced.

Note that, in addition to the surface modification technique, the post-modification treatment is also important to the defiltration behavior. If after the gas–solid treatment the MCM-41 particles are not vacuum dried but simply dried in air for 6 h, liquid defiltration can be largely suppressed. As shown in Fig. 4, while in the first loading cycle the infiltration plateau is quite evident, at the second loading little infiltration can be observed, which suggests that during unloading in the first cycle most of the confined liquid does not defiltrate. The occupied nanopores are deactivated and cannot participate in the infiltration in the second cycle. This should be attributed to the impurities of HCl that cannot be fully removed by air drying. They can create concentration sites of water molecules, making the energy barrier to defiltration much larger. During vacuum drying, since HCl is quite evaporable, it can be nearly fully removed, and thus the measured sorption curve reflects the intrinsic properties of chlorotrimethylsilane-modified MCM-41.

4. Concluding remarks

In summary, gas–solid reaction method can be employed to surface treat MCM-41. Due to the high molecular mobility in vapor phase, the surface group distribution is quite uniform. Compared with liquid–solid-treated material, the infiltration pressure

of gas–solid-treated MCM-41 is slightly higher, while the hysteresis of sorption curve is much less pronounced. Therefore, it can work more smoothly for continuous energy absorption. The liquid composition and the post-modification treatment procedure are also of important effects on infiltration and defiltration behaviors.

Acknowledgements

This study was supported by the Sandia National Lab and the National Science Foundation under Grant No. CMS-0623973.

References

[1] V. Eroshenko, R.C. Regis, M. Soulard, J. Patarin, Energetics—a new field of applications for hydrophobic zeolites, J. Am. Chem. Soc. 123 (2001) 8129.
[2] V.D. Borman, A.A. Belogorlov, A.M. Grekhov, V.N. Tronin, V.I. Troyan, Observation of dynamic effects in the percolation transition in a nonwetting-nanoporous body system, JETP Lett. 74 (2001) 258.
[3] A. Han, Y. Qiao, A volume memory liquid, Appl. Phys. Lett. 91 (2007) 173123.
[4] Z.G. Wei, R. Sandstrom, S. Miyazaki, Shape-memory materials and hybrid composites for smart systems. Pt. I. Shape-memory materials, J. Mater. Sci. 33 (1998) 3743.
[5] A.Y. Fadeev, V.A. Eroshenko, Study of penetration of water into hydrophobized porous silicas, J. Colloid Interf. Sci. 187 (1997) 275.
[6] T. Martin, B. Lefevre, D. Brunel, A. Galarneau, F. Di Renzo, F. Fajula, P.F. Gobin, J.F. Quinson, G. Vigier, Dissipative water intrusion in hydrophobic MCM-41 type materials, Chem. Commun. (2002) 24.
[7] Y. Qiao, X. Kong, Modeling of the kinetics of confined nonwetting flow in a mesoporous particle, Phys. Scripta 71 (2005) 27.
[8] X. Kong, Y. Qiao, Improvement of recoverability of a nanoporous energy absorption system by using chemical admixture, Appl. Phys. Lett. 87 (2005) 163111.
[9] A. Han, Y. Qiao, Suppression effect of liquid composition on defiltration of nanofluids in lyophobic environment, J. Phys. D: Appl. Phys. 40 (2007) 3436.
[10] M.A. Thomas, M. Thommes, Characterization of Porous Solids and Powders—Surface Area, Pore Size and Density, Springer, 2006.
[11] V.D. Borman, A.M. Grekhov, V.I. Troyan, Investigation of the percolation transition in a nonwetting liquid-nanoporous medium system, J. Exp. Theor. Phys. 91 (2000) 170.
[12] A. Han, X. Kong, Y. Qiao, Pressure induced infiltration in nanopores, J. Appl. Phys. 100 (2006) 014308.
[13] Y. Qiao, G. Cao, X. Chen, Effects of gas molecules on nanofluidic behaviors, J. Am. Chem. Soc. 129 (2007) 2355.
[14] V.K. Punyamurtula, A. Han, Y. Qiao, Damping properties of nanoporous carbon–cyclohexane mixtures, Adv. Eng. Mater. 9 (2007) 209–211.
[15] X. Kong, F.B. Surani, Y. Qiao, Effects of addition of ethanol on the infiltration pressure of a mesoporous silica, J. Mater. Res. 20 (2005) 1042–1045.
[16] F.B. Surani, Y. Qiao, Pressure induced liquid infiltration in a functionalized poly(acrylic acid-co acrylamide) potassium salt gel matrix material, Mater. Res. Innov. 10 (2006) 129–137.
[17] G. Lu, T. Yu, Energy Absorption of Structures and Materials, CRC Press, 2003.
[18] X. Kong, Y. Qiao, Improvement of recoverability of a nanoporous energy absorption system by using chemical admixture, Appl. Phys. Lett. 86 (2005) 151919.1–151919.3.
[19] X. Kong, F.B. Surani, Y. Qiao, Energy absorption of nanoporous silica particles in aqueous solutions of sodium chloride, Phys. Scripta 74 (2006) 531–534.
[20] F.B. Surani, Y. Qiao, Pressure induced infiltration of an epsomite-silica system, Phil. Mag. Lett. 86 (2006) 253–260.
[21] F.B. Surani, X. Kong, Y. Qiao, Two-staged sorption isotherm of a nanoporous energy absorption system, Appl. Phys. Lett. 87 (2005) 251906.1–251906.3.
[22] A. Han, Y. Qiao, Pressure induced infiltration of aqueous solutions of multiple promoters in a nanoporous silica, J. Am. Chem. Soc. 128 (2006) 10348–10349.
[23] J.A. Schwarz, C.I. Contescu, Surfaces of Nanoparticles and Porous Materials, CRC Press, 1999.
[24] A. Han, Y. Qiao, Effects of surface treatment of a MCM-41 on motions of confined liquids, J. Phys. D: Appl. Phys. 40 (2007) 5743–5746.
[25] M.H. Lim, A. Stein, Comparative studies of grafting and direct syntheses of inorganic–organic hybrid mesoporous materials, Chem. Mater. 11 (1999) 3285.
[26] C.W. Jones, M. Tsapatsis, T. Okubo, M.E. Davis, Organic-functionalized molecular sieves. III. Shape selective catalysis, Micropor. Mesopor. Mater. 42 (2005) 21.
[27] T. Asefa, C. Yoshina-Ishii, M.J. MacLachlan, G.A. Ozin, New nanocomposites—putting organic function inside the channel walls of periodic mesoporous silica, J. Mater. Chem. 10 (2000) 1751.
[28] A. Han, Y. Qiao, Controlling infiltration pressure of a nanoporous silica gel via surface treatment, Chem. Lett. 36 (2007) 882–883.
[29] D. Leyden, Silylated Surfaces, Routledge, 1980.
[30] F.B. Surani, X. Kong, D.B. Panchal, Y. Qiao, Energy absorption of a nanoporous system subjected to dynamic loadings, Appl. Phys. Lett. 87 (2005) 163111.1–163111.3.
[31] Y. Qiao, X. Kong, S.S. Chakravarthula, An analysis of aggregate response of confined liquid in nanoenvironment, J. Math. Chem. 37 (2005) 93–99.
[32] M.P. Allen, D.J. Tildesley, Computer Simulation of Liquids, Oxford Science Publications, 1990.
[33] F.B. Surani, Y. Qiao, An energy absorbing polyelectrolyte gel matrix composite material, Compos. Part A 37 (2006) 1554–1556.
[34] F.B. Surani, Y. Qiao, Infiltration and defiltration of an electrolyte solution in nanopores, J. Appl. Phys. 100 (2006) 034311.1–034311.4.